ACS APPLIED MATERIALS & INTERFACES

RESEARCH ARTICLE

www.acsami.org

Hierarchical Nanostructures of Copper(II) Phthalocyanine on Electrospun TiO_2 Nanofibers: Controllable Solvothermal-Fabrication and Enhanced Visible Photocatalytic Properties

Mingyi Zhang,[†] Changlu Shao,[*,†] Zengcai Guo,[‡] Zhenyi Zhang,[†] Jingbo Mu,[‡] Tieping Cao,[†,§] and Yichun Liu[†]

[†]Center for Advanced Optoelectronic Functional Materials Research and Key Laboratory of UV Light-Emitting Materials and Technology of Ministry of Education, and [‡]Department of Chemistry, Northeast Normal University, 5268 Renmin Street, Changchun 130024, People's Republic of China

[§]Department of Chemistry, Baicheng Normal College, Baicheng, Jilin 137000, People's Republic of China

ABSTRACT: In the present work, 2,9,16,23-tetranitrophthalocyanine copper(II) (TNCuPc)/TiO_2 hierarchical nanostructures were successfully fabricated by a simple combination method of electrospinning technique and solvothermal processing. Scanning electron microscopy (SEM), energy-dispersive X-ray (EDX) spectroscopy, X-ray diffraction (XRD), UV−vis diffuse reflectance (DR), Fourier transform infrared spectrum (FT-IR), X-ray photoelectron spectroscopy (XPS), and thermal gravimetric and differential thermal analysis (TG-DTA) were used to characterize the as-synthesized TNCuPc/TiO_2 hierarchical nanostructures. The results showed that the secondary TNCuPc nanostructures were not only successfully grown on the primary TiO_2 nanofibers substrates but also uniformly distributed without aggregation. By adjusting the solvothermal fabrication parameters, the TNCuPc nanowires or nanoflowers were facilely fabricated, and also the loading amounts of TNCuPc could be controlled on the TNCuPc/TiO_2 hierarchical nanostructural nanofibers. And, there might exist the interaction between TNCuPc and TiO_2. A possible mechanism for the formation of TNCuPc/TiO_2 hierarchical nanostructures was suggested. The photocatalytic studies revealed that the TNCuPc/TiO_2 hierarchical nanostructures exhibited enhanced photocatalytic efficiency of photodegradation of Rhodamine B (RB) compared with the pure TNCuPc or TiO_2 nanofibers under visible-light irradiation.

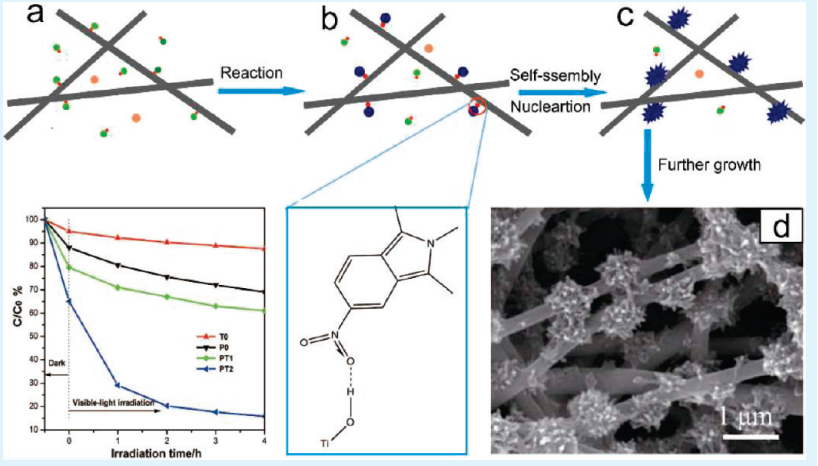

KEYWORDS: TiO_2, phthalocyanine, electrospinning, solvothermal, hierarchical nanostructures, photocatalysis

1. INTRODUCTION

Titanium dioxide has been widely studied as a semiconductor photocatalyst for potential application in air purification and water treatment because of its high oxidative power, photostability, and nontoxicity.[1−3] However, one severe disadvantage of this semiconductor material is the large band gap of 3.2 eV for anatase form, which limits its photoresponse to the ultraviolet (UV) region. Unfortunately, only a very small fraction (3−5%) of the solar spectrum falls in the UV region.[4] To efficiently utilize solar energy, many attempts have been undertaken to make TiO_2 responsive to visible light, such as dye-sensitization,[5−7] metal complex sensitization,[8−10] coupling with a small band gap semiconductor,[11−13] and doping transitional metal ions or nonmetal atoms,[14−22] and so on. In these methods, the organic dye photosensitization has proved to be an inexpensive and efficient method to extend the absorption spectra of TiO_2 into the visible region. In this approach, a dye molecule can absorb visible light to produce a singlet or triplet state (dye*). An electron is then injected from the singlet or triplet excited state of the dye into the conduction band (CB) of TiO_2. The injected electron can reduce surface chemisorbed O_2 to yield strong oxidizing radicals (such as $O_2\bullet^-$, $HO_2\bullet$, $OH\bullet^-$), which can degrade the organic pollutants. Among these dyes, metallophthalocyanines (MPc), as a typical organic semiconductors, have been extensively investigated in organic dye photosensitization, because of its nontoxicity, low processing cost, high thermal and chemical stability, and intensive absorption in the visible-light region.

Received: October 13, 2010
Accepted: December 7, 2010
Published: January 10, 2011

Table 1. Experimental Conditions, TNCuPc Nanostructure Characteristics, And Chemical Component of the Prepared Samples

	precursors				
sample	$Cu(OAc)_2$ (mM)	4-nitrophthalonitrile (mM)	TiO_2 nanofibers (mg)	morphology	TNCuPC/TiO_2molar ratio [a]
PT1	0.025	0.1	15	nanowires	1:(49 ± 3)
PT2	0.125	0.5	15	nanoflowers	1:(21 ± 3)
P0	0.125	0.5	0		

[a] The value is determined by EDX.

Recently, a rich variety of methods such as sol−gel, spin coating, hydrothermal, immersion method, and so forth have been demonstrated to prepare nanostructural MPc sensitized TiO_2 photocatalyst, including nanoparticles, films, and so on.[23−27] Among these materials, the MPc-sensitized TiO_2 nanoparticles exhibited a high photocatalytic activity because of their high surface area. However, it is often limited, because the suspended particulate catalysts are easily lost in the process of photocatalytic reaction and separation, which may repollute the treated water again. Meanwhile, the MPc-sensitized TiO_2 films can be fixed and reclaimed easily, but their photocatalytic activity is decreased because of their low surface area. Compared with the corresponding nanoparticles and thin films of MPc-sensitized TiO_2, the one-dimensional nanomaterials of the MPc-sensitized TiO_2 possessed high photocatalytic activity and favorable recycling characteristics due to its high surface area and one-dimensional properties, which might be deemed as potential good candidates for practical application. However, to the best of knowledge, there has been no report on the preparation and photocatalytic properties of these kinds of materials.

In the present paper, we report a successful attempt at the fabrication of 2,9,16,23-tetranitrophthalocyanine copper(II) (TNCuPc) nanostructure grown on the electrospun TiO_2 nanofibers through solvothermal processing. The as-prepared TNCuPc/TiO_2 hierarchical nanostructure exhibited excellent photocatalytic activity as compared with the pure electrospun TiO_2 nanofiber and TNCuPc under visible-light irradiation. Moreover, the one-dimensional hierarchical nanostructures of TNCuPc/TiO_2 could be reclaimed easily by sedimentation without a decrease in the photocatalytic activity due to the one-dimensional properties. Also, the interactions between TNCuPc molecules and TiO_2 through the nitro groups of TNCuPc and the hydroxyl group of TiO_2 in the TNCuPc/TiO_2 hierarchical nanostructure could make the TNCuPc load stably on the surface of TiO_2 nanofibers.

2. EXPERIMENTAL SECTION

2.1. Preparation of TiO_2 Nanofibers. First, 2 g of poly(vinyl pyrrolidone) powder (PVP, M_w = 1 300 000) was added to a mixture of 9 mL of absolute ethanol and 5 mL of acetic acid in a capped bottle. The obtained solution was stirred for 1 h to generate a homogeneous solution. Then, 2.0 g $Ti(OC_4H_9)_4$ was added to the solution, and the mixture was continuously stirred for another 1 h to make precursor solution. Three milliliters of the precursor solution was placed in a 5 mL syringe equipped with a blunt metal needle of 0.8 mm outer diameter and 0.6 mm inner diameter. A stainless steel plate covered with a sheet of aluminum foil was employed as the collector. The distance between the needle tip and collector was 15 cm, and the voltage was set at 9 kV. The as-collected nanofibers were calcined at 550 °C for 2 h to form anatase TiO_2 nanofibers.

2.2. Fabrication of TNCuPc/TiO_2 Hierarchical Nanostructures. In a typical experiment, 4-nitrophthalonitrile (0.100 mmol), $Cu(OAc)_2 \cdot 2H_2O$ (0.025 mmol), ammonium molybdate (1 mg), and TiO_2 nanofibers (15 mg) were put into a Teflon-lined stainless steel autoclave of 25 mL capacity that contained 20 mL of ethylene glycol solution. The mixture was then stirred to form a milklike suspension, sealed, and solvothermally treated at 160 °C for 72 h. The autoclave was then cooled to room temperature. The obtained composite nanofibers was washed with deionized water and ethanol to remove any ionic residual then dried in oven at 80 °C for 4 h. The as-fabricated sample was denoted as PT1. By tuning the precursor concentration for synthesizing TNCuPc, another sample of TNCuPc/TiO_2 was fabricated and was denoted as PT2. And the TNCuPc synthesized in the absence of TiO_2 nanofibers was denoted as P0. The detailed experimental conditions for the fabrication of PT1 and PT2 were listed in Table 1. In addition, for simplicity, pure TiO_2 nanofibers were denoted as T0.

2.3. Characterization. Field-emission scanning electron microscope (FESEM, XL-30 ESEM FEG, Micro FEI Philips) was used to observe morphology of the samples. Energy-dispersive X-ray (EDX) spectroscopy being attached to scanning electron microscopy (SEM) was used to analyze the composition of samples. X-ray diffraction (XRD) patterns of the samples were recorded on a Rigaku, D/max-2500 X-ray diffractometer. The UV−vis diffuse reflectance (DR) spectroscopy of the samples were recorded on a Cary 500 UV−vis−NIR spectrophotometer. Fourier transform infrared spectra (FT-IR) were obtained on Magna 560 FT-IR spectrometer with a resolution of 1 cm^{-1}. X-ray photoelectron spectroscopy (XPS) was performed on a VG-ESCALAB LKII instrument with Mg Kα ADES ($h\nu$ = 1253.6 eV) source at a residual gas pressure of below 1 × 10^{-8} Pa. Thermal gravimetric and differential thermal analysis (TG-DTA) was carried out on a NETZSCH STA 449C thermoanalyzer in a N_2 atmosphere.

2.4. Photocatalytic Test. The photoreactor was designed with an internal xenon lamp (XHA 150W) equipped with a cutoff glass filter transmitting λ > 400 nm surrounded by a water-cooling quartz jacket to cool the lamp, where 100 mL of the RB solution with an initial concentration of 10 mg L^{-1} in the presence of solid catalyst (0.1 g). The solution was stirred in the dark for 30 min to obtain a good dispersion and reach adsorption−desorption equilibrium between the organic molecules and the catalyst surface. Decreases in the concentrations of dyes were analyzed by a Cary 500 UV−vis−NIR spectrophotometer at λ = 554 nm. At given intervals of illumination, the samples (3 mL) of the reaction solution were taken out and then centrifuged and filtered. Finally, the filtrates were analyzed.

3. RESULTS AND DISCUSSION

3.1. Scanning Electron Microscopy (SEM) Images and the Corresponding Energy-Dispersive X-ray (EDX) Spectra. Figure 1 showed the typical scanning electron microscopy (SEM) images and the corresponding energy-dispersive X-ray (EDX) spectra of the pure TiO_2 nanofibers (T0) and the TNCuPc/TiO_2 hierarchical nanostructures (PT1 and PT2). Images A and B in Figure 1 present the SEM images of the as-electrospun TiO_2 nanofibers (T0) with the low and high magnification, respectively. It could be seen that the lengths of these randomly oriented nanofibers could reach several micrometers, and the diameters of those nanofibers ranged from 250 to 350 nm after calcinations at 550 °C. Furthermore, the surface of pure TiO_2 nanofibers (T0) was smooth. However, as observed in images D and E and G and H in Figure 1, it was found that two kinds of TNCuPc nanostructure

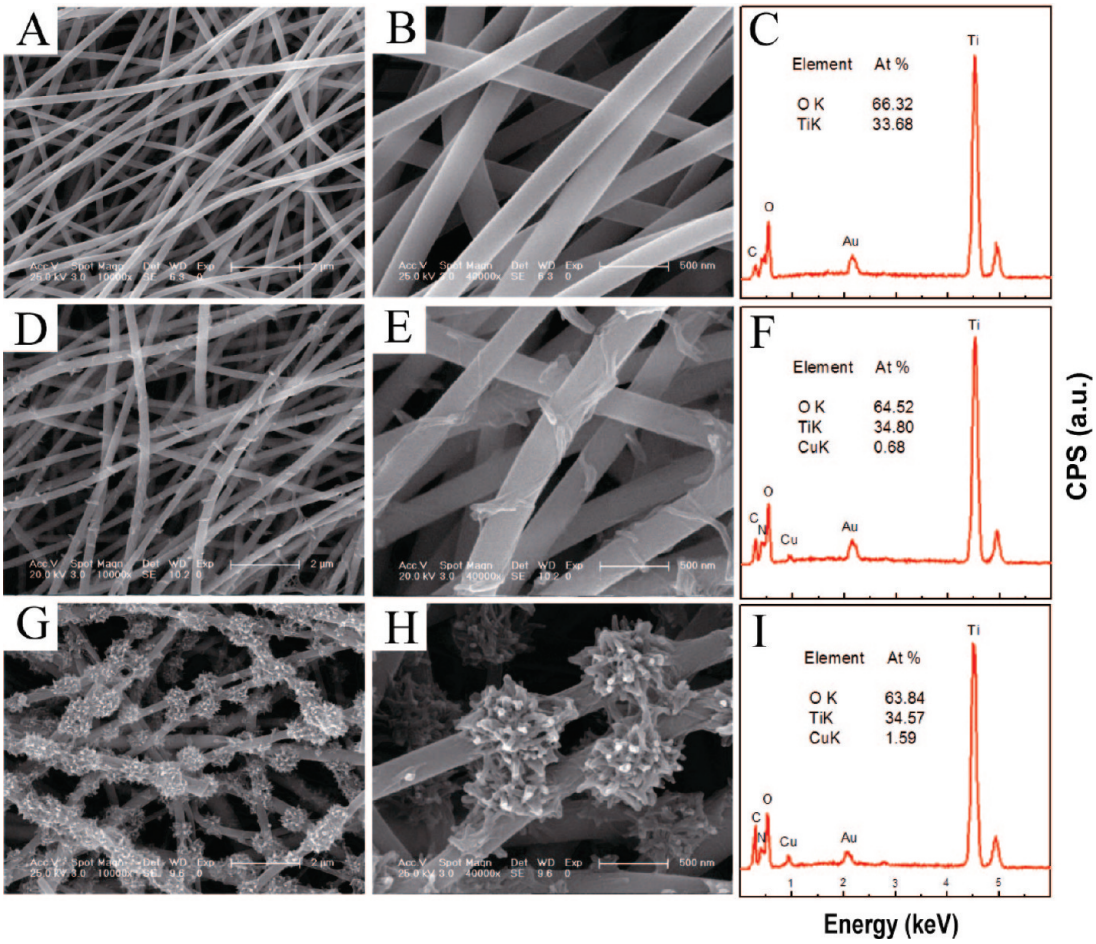

Figure 1. (A) Low-magnification SEM image of sample T0. (B) High-magnification SEM image of the sample T0. (C) EDX spectrum of sample T0. (D) Low-magnification SEM image of sample PT1. (E) High-magnification SEM image of sample PT1. (F) EDX spectrum of sample PT1. (G) Low-magnification SEM image of sample PT2. (H) High-magnification SEM image of the sample PT2. (I) EDX spectrum of sample PT2.

grew on the surface of TiO_2 nanofibers after solvothermal reaction for 72 h. Images D and E in Figure 1 show images of solvothermal treated TiO_2 nanofibers (PT1) with the low and high magnification, respectively. From Figure 1D, it was found that a lot of TNCuPc nanowires uniformly grew twining on the surface of TiO_2 nanofibers. Meanwhile, the TNCuPc nanowires possessed an average length of about 300 nm and a diameter of less than 50 nm (Figure 1E). By appropriately tuning the precursor concentration during solvothermal reaction, the morphology of TNCuPc nanostructures grown on TiO_2 nanofibers changed from the nanowires (PT1) to nanoflowers (PT2). As shown in Figure 1G, it could be observed that a number of TNCuPc nanoflowers instead of nanowires were grown on the surface of TiO_2 nanofiber surface and the nanoflowers appeared to distribute uniformly. In Figure 1H, it appeared that nanoflowers on the TiO_2 nanofibers were composed of a large number of nanorods, which radially grew from the center. The nanorods had diameters of 30−60 nm and lengths of 80−120 nm. Meanwhile, panels C, F and I in Figure 1show the energy-dispersive X-ray (EDX) spectra from images A, D and G in Figure 1, respectively. It was indicated that Ti, O, and C elements existed in pure TiO_2 electropun nanofibers, whereas Ti, Cu, O, N, and C existed in TNCuPc/TiO_2 hierarchical nanostructures (PT1 and PT2), respectively. In addition, the EDX analysis indicated that the atomic ratio of Cu to Ti was 1:(49 ± 3) for PT1 and 1:(21 ± 3) for PT2, respectively, confirming the uniformity of the TNCuPc nanostructures successfully grown on the surface of TiO_2 nanofibers.

3.2. X-ray Diffraction (XRD) Patterns. The X-ray diffraction (XRD) patterns of the pure TiO_2 nanofibers (T0) and TNCuPc/TiO_2 hierarchical nanostructures (PT1 and PT2) were shown in Figure 2. As observed in Figure 2a, six reflection peaks appeared at 2θ = 25.4° (101), 37.9° (004), 48.0° (200), 53.8° (105), 54.9° (211), and 62.8° (204), respectively, which were attributabled to the anatase TiO_2 (JCPDS, No. 21−1272). The diffraction peaks of the TiO_2 nanofibers were sharp and intense, indicating the highly crystalline character of the nanofibers. As for the TNCuPc/TiO_2 hierarchical nanostructures (Figure 2b, c), except the diffraction peaks of anatase TiO_2, all other peaks located at 13.9, 22.5, and 27.2° could be indexed to the diffraction peaks of TNCuPc.[28] Notably, in curves b and c in Figure 2, the diffraction peaks of the TNCuPc were broad and weak, indicating a small crystal size or a poor crystallinity of TNCuPc in the TNCuPc/TiO_2 hierarchical nanostructures. These results suggested that the TNCuPc nanostructure had been formed on the TiO_2 nanofibers by solvothermal processing.

3.3. UV−Vis Diffuse Reflectance Spectra. The UV−Vis diffuse reflectance spectra of the pure TiO_2 nanofibers (T0), TNCuPc/TiO_2 hierarchical nanostructures (PT1 and PT2), and TNCuPc (P0) were shown in Figure 3. As observed in Figure 3a, the diffuse reflectance spectrum of TiO_2 nanofibers only exhibited

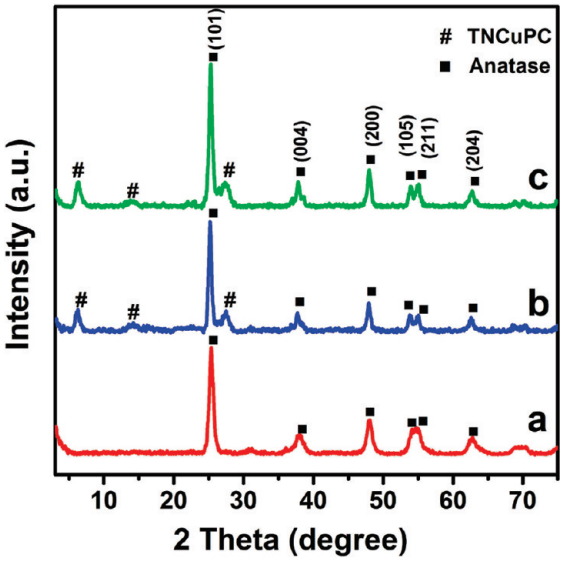

Figure 2. XRD patterns of sample T0 (curve a), PT1 (curve b), and PT2 (curve c).

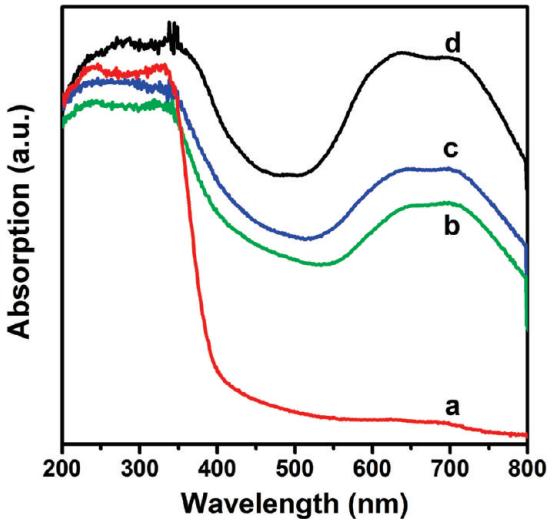

Figure 3. UV−vis diffuse reflectance spectra of the sample T0 (curve a), PT1 (curve b), PT2 (curve c), and P0 (curve d).

the fundamental absorption band in the UV region, there was no more absorption in visible wavelengths. In curves b and c in Figure 3, TNCuPc/TiO_2 hierarchical nanostructures (PT1 and PT2) exhibited absorption bands in the wavelengths of 600−750 nm that might be attributable to the Q-band of TNCuPc.[29] The Q-band corresponds to excitation between the ground state a_{1u} (π) HOMO to e_g (π^*) LUMO. Furthermore, two splitting absorption bands are observed around 630 and 710 nm, which is likely due to the vibronic coupling in the excited state.[30−32] These absorption bands between of 600−750 nm was also observed in the UV−Vis diffuse reflectance spectrum of pure TNCuPc (P0) (Figure 3d). The above results indicated that the sensitization of TiO_2 with TNCuPc could extend the absorbance spectrum of TiO_2 into visible region.

3.4. Fourier Transform Infrared (FT-IR) Spectra. The FT-IR spectra of the pure TiO_2 nanofibers (T0), TNCuPc/TiO_2 hierarchical nanostructures (PT1 and PT2), and TNCuPc (P0) were shown in Figure 4. As observed in Figure 4a, the FT-IR spectrum of

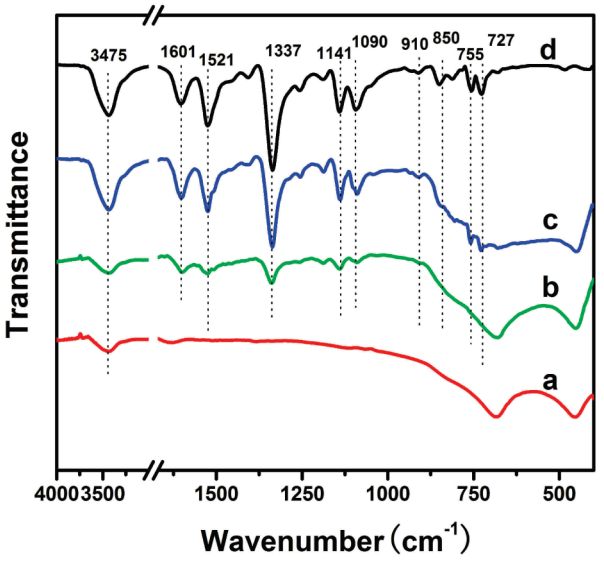

Figure 4. FT-IR spectra of the sample T0 (curve a), PT1 (curve b), PT2 (curve c), and P0 (curve d).

the TiO_2 nanofibers only exhibited the absorption peaks around 450 cm^{-1} and 680 cm^{-1} which was assigned to the Ti−O vibration. No characteristic peaks for impurity were observed, indicating that all the organic molecules could be removed completely from the PVP/Ti$(OC_4H_9)_4$ composite fibers after calcination at 550 °C, and the pure TiO_2 nanofibers was obtained at this temperature. From the Figure 4b and c, it was observed that the TNCuPc/TiO_2 hierarchical nanostructures appeared several absorption peaks at around 727, 755, 910, 1090, 1141, and 1605 cm^{-1}, which might be assigned to phthalocyanine skeletal and metal−ligand vibrations, respectively.[33,34] And, the other absorption peaks at 1521, 1337, and 850 cm^{-1} may be assigned to the asymmetric N−O stretching, symmetric N−O stretching and C−NO_2 stretching due to the nitro groups present in the structure of the TNCuPc molecule.[28] And, these peaks were also observed in the FT-IR spectrum of pure TNCuPc (P0) (Figure 4d). The above results revealed that TNCuPc is synthesized successfully on the surface of TiO_2 nanofibers.

3.5. X-ray Photoelectron Spectroscopy (XPS) Spectra. The chemical composition and purity of the TNCuPc/TiO_2 hierarchical nanostructures (PT2) was studied and compared with that of the TiO_2 nanofibers(T0) by XPS analysis. The fully scanned spectra (Figure 5a) demonstrate that Ti, O, and C elements existed in pure TiO_2 nanofibers, while Ti, Cu, O, N, and C existed in TNCuPc/TiO_2 hierarchical nanostructures, respectively. The C element of TiO_2 nanofibers can be ascribed to the adventitious carbon-based contaminant. The high resolution XPS spectra with scanning over the following areas are analyzed: the binding energies for the Ti 2p region around 460 eV, the Cu 2p region around 940 eV, and the O1s region around 530 eV. As shown in Figure 5b, there are two peaks in the Ti 2p region. The peak located at 464.2 eV corresponds to the Ti $2p_{1/2}$ and another one located at 458.5 eV is assigned to Ti $2p_{3/2}$. The splitting between Ti $2p_{1/2}$ and Ti $2p_{3/2}$ is 5.7 eV, indicating a normal state of Ti^{4+} in the as-prepared TNCuPc/TiO_2 hierarchical nanostructures. Besides, the peaks for Ti 2p in the sample PT2 showed no shift compared with that in pure TiO_2 nanofibers, confirming that the structure of TiO_2 remained intact after synthesis of TNCuPc nanoparticles. As observed in Figure 5c, there were two symmetric peaks in the Cu

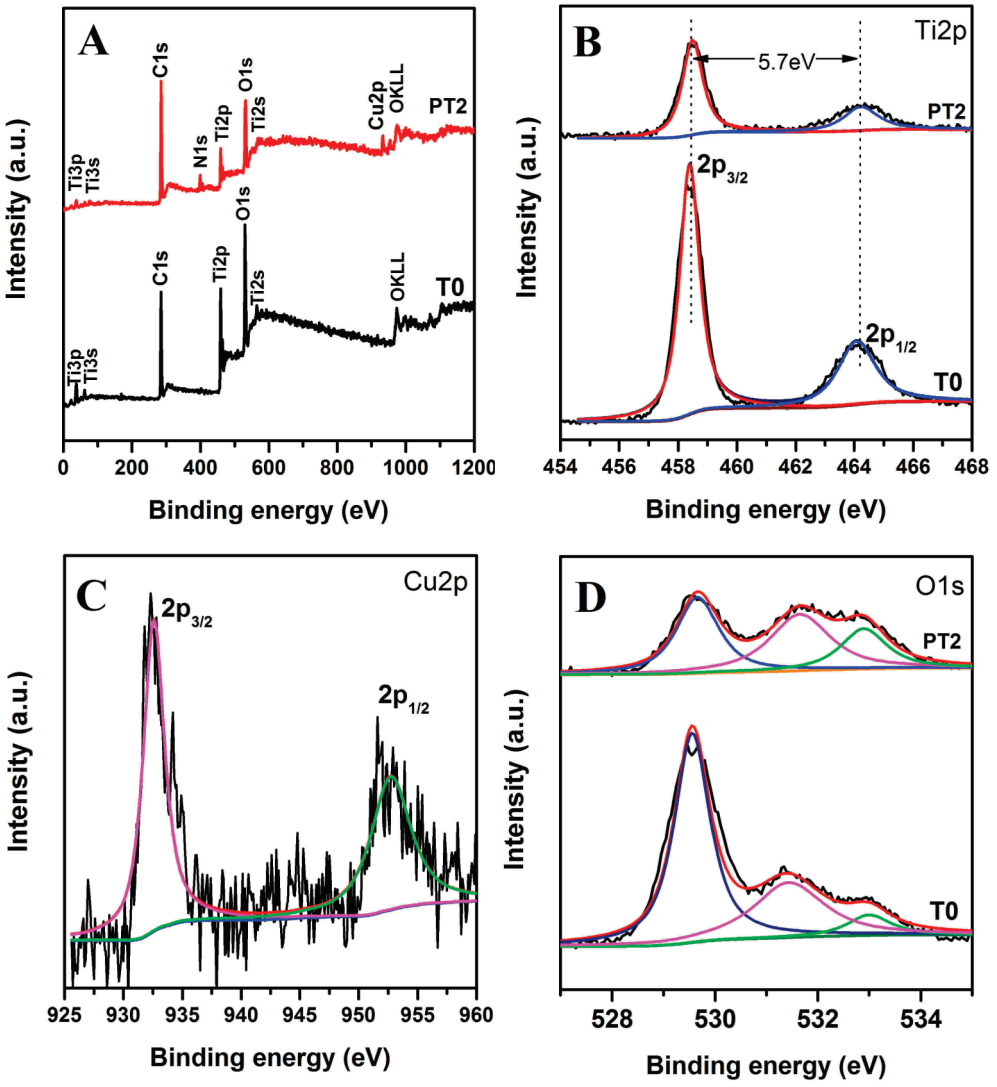

Figure 5. (A) XPS fully scanned spectra of the sample T0 and PT2; (B) XPS spectra of Ti 2p for the sample T0 and PT2; (C) XPS spectrum of Cu 2p for the sample PT2; (D) XPS spectra of O1s for the sample T0 and PT2.

2p region. The peak centered at 933.1 eV corresponded to the Cu $2p_{3/2}$ and another one centered at 953.2 eV was assigned to Cu $2p_{1/2}$, indicating a normal state of Cu^{2+} in the TNCuPc molecule. Figure 5d presented the O1s photoelectron peaks. The shape of a wide and asymmetric peak of O 1s spectrum indicated that there could be more than one chemical state according to the binding energy. It included crystal lattice oxygen (O_{Ti-O}), surface hydroxyl groups (O_{OH}), and adsorbed water with increasing binding energy. Using the XPS Peak fitting program, version 4.1, each O1s XPS spectrum is fitted to three kinds of chemical states. After calculation, the apparent O_{OH}/O_{Ti-O} ratio is determined to be 0.49 for the sample PT2, which is three-times higher than that of sample T0. Thus, it can be deduced that the amounts of surface OH groups on the surface of the TNCuPc/TiO_2 hierarchical nanostructures (PT2) are significantly increased by the sensitization of TNCuPc based on the analyses of XPS. In addition, FT-IR spectra (Figure 4) were also further utilized to detect the surface OH groups and water adsorption on the surface of the sample. For the TNCuPc/TiO_2 hierarchical nanostructures (PT2), an overlapped broad peak of high intensity at 3475 cm^{-1} is observed, which is characterized as surface Ti−OH and hydrogen-bonded molecular H_2O species. On the other hand, for the pure TiO_2 nanofibers, the intensity of the surface hydroxyl group band at 3475 cm-1 is significantly decreased compared with that of the TNCuPc/TiO_2 hierarchical nanostructures. The increasing amount of surface hydroxyl group in the TNCuPc/TiO_2 hierarchical nanostructures (PT2) may originate from the high dispersion and hygroscopic nature of the TNCuPc nanostructure (PT2). In fact, it has been reported that Metallophthalocyanines (MPc) and their derivatives has been used as a moisture sensor for this reason.[35,36] As we all known, an important factor for the efficient photooxidation of organic substrates would depend on the concentration of OH• radicals by photooxidation of surface hydroxyl groups.[37] The significantly increased surface hydroxyl groups might enhance the photocatalytic of TNCuPc/TiO_2 hierarchical nanostructures.

3.6. Thermal Analysis (TG/DTA). Figure 6 showed the TG and DTA curves of the pure TiO_2 nanofibers (T0), TNCuPc/TiO_2 hierarchical nanostructures (PT2) and TNCuPc (P0). As observed in the TG curve in Figure 6, the TiO_2 nanofibers did not show a significant weight-loss step, suggesting that the TiO_2 nanofibers did not decompose in N_2 atmosphere. And, the TNCuPc/TiO_2 hierarchical nanostructures (PT2) appeared to have one significant

dx.doi.org/10.1021/am100989a |ACS Appl. Mater. Interfaces 2011, 3, 369–377

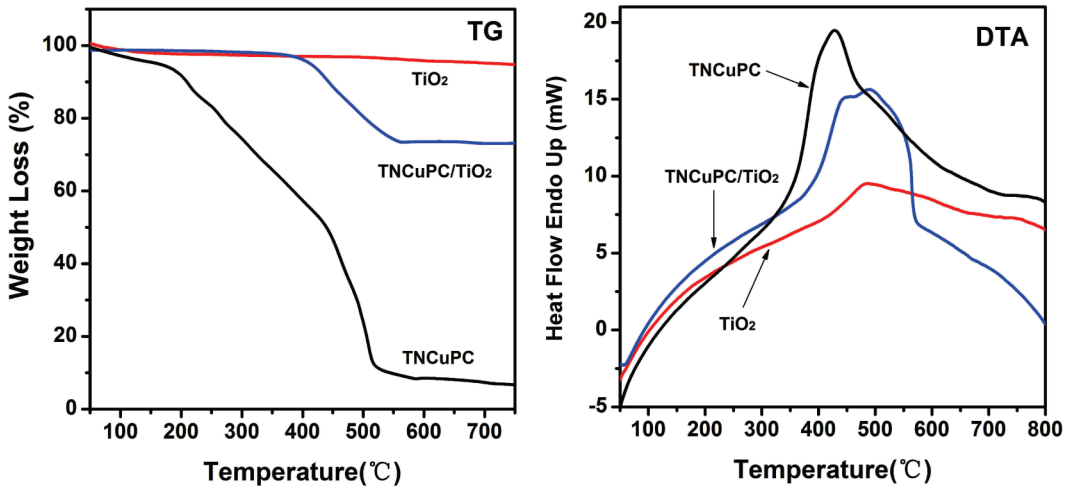

Figure 6. TG-DTA curves of thermal decomposition of samples T0, PT2, and P0.

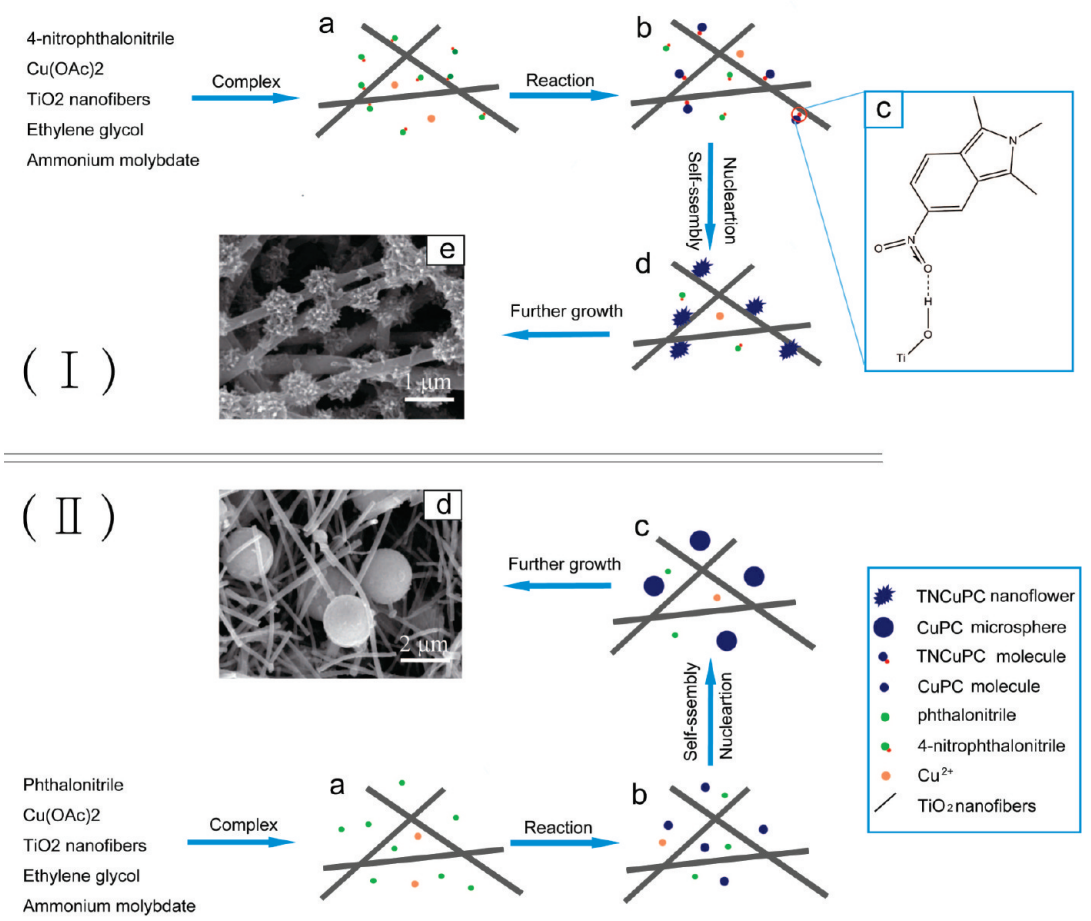

Figure 7. Possible mechanism for the formation of TNCuPc/TiO_2 hierarchical nanostructures(I)and CuPC/TiO2 compound(II).

weight loss at 380−560 °C, which might be attributed to the decomposition of TNCuPc on the TiO_2 nanofibers surfaces. The weight loss could be used to estimate the weight percentage of TNCuPc attached to the TiO_2 nanofibers. From Figure 6, the weight percentage of attached TNCuPc in the TNCuPc/TiO_2 hierarchical nanostructures was determined to be about 25%, corresponding to the results of the EDX spectrum in Figure 1I. As for the pure TNCuPC, it was showed two major weight-loss steps from 50 to 180 °C and from 180 to 520 °C, which might be due to the loss of moisture and the decomposition of TNCuPc, respectively. Obviously, the decomposition temperature of the pure TNCuPC was significantly lower than the TNCuPc which grew on the TiO_2 nanofibers surfaces. On the other hand, the DTA curve of TiO_2 nanofibers exhibited the exothermic peaks around 483 °C, which should be assigned to the phase transformation from anatase TiO_2 to rutile TiO_2. And, the DTA curve of the pure TNCuPc

dx.doi.org/10.1021/am100989a |ACS Appl. Mater. Interfaces 2011, 3, 369–377

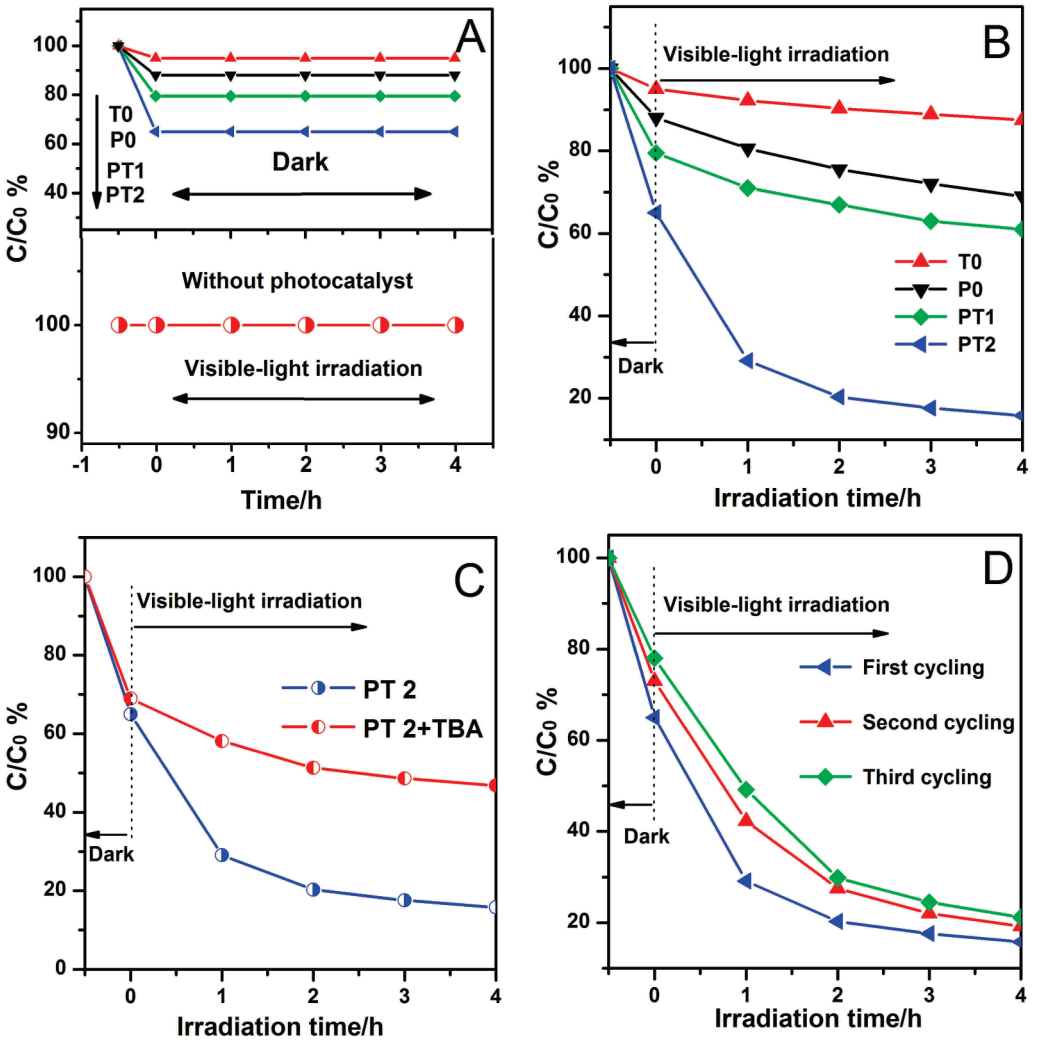

Figure 8. (A) Degradation profiles of RB in the presence of the PT1 and PT2 nanofiber photocatalysts but in the dark and with visible light irradiation but in the absence of the nanofiber photocatalysts. (B) Degradation profiles of RB over different samples (C_0 = 10 mg/L, T0, PT1, PT2 = 0.1 g, P0 = 0.025 g). (C) Effect of tert-butyl alcohol (TBA) on the photocatalytic degradation of RB for the sample PT2. (D) Photocatalytic activity of the sample PT2 for RB degradation with three times of cycling uses.

exhibited an exothermic peaks around 427 °C because of its decomposition. However, the DTA curve of the TNCuPc/TiO_2 hierarchical nanostructures exhibited two exothermic peaks at around 446 and 491 °C, which might be assigned to the decomposition of TNCuPc and the phase transformation from anatase TiO_2 to rutile TiO_2. Obviously, the two exothermic peaks clear shifted toward the high temperature contrast with the pure TNCuPc and pure TiO_2 nanofibers. The above results illuminated that interactions between the TNCuPc and TiO_2 nanofibers probably exist, suggesting that the TNCuPc was stably loaded on the surface of TiO_2 nanofibers in the TNCuPc/TiO_2 hierarchical nanostructures.

3.7. Formation Mechanism. On the basis of the above results, a possible mechanism for the formation of TNCuPc/TiO_2 hierarchical nanostructures was suggested (Figure 7I). As shown in Figure 7I, at the early stage, the 4-nitrophthalonitrile uniformly distribute in the TiO_2 nanofibers through the interaction of hydrogen bonds, which formed by the nitro groups of 4-nitrophthalonitrile and the surface hydroxyl groups of TiO_2 nanofibers (Figure.7Ia). Subsequently, 4-nitrophthalonitrile reacted with $Cu(OAc)_2$ to in situ synthesize TNCuPc molecules. The TNCuPc molecules became the nuclei and quickly grew into the primary seeds on the surface of the TiO_2 nanofibers through the hydrogen bonds (Figure.7Ib and c). In the following secondary growth stage, the primary TNCuPc seeds would aggregated into nanoflowers on the surface of TiO_2 nanofibers (Figure.7Id). Finally, after further growth, the TNCuPc/TiO_2 hierarchical nanostructured was prepared (Figure.7Ie). Obviously, the nitro groups of TNCuPc played a significant role in the whole reaction system to form the TNCuPc/TiO_2 hierarchical nanofibers. To further clarify the formation mechanism, we tried to prepare non-nitro-substituted copper phthalocyanine (CuPC)/TiO_2 nanofibers with phthalonitrile instead of 4-nitrophthalonitrile. However, it was found that no hierarchical nanostructure was formed; instead, the CuPC was so prone to form congeries in solution that they congregated larger microspheres with diameter about 2 μm (Figure 7IId). In sharp contrast with the secondary TNCuPc nanoflowers, the CuPC prepared through the same way could not grow on the surface of TiO_2 nanofibers because of the absence of nitro group. These observations further indicated that nitrogroups played a significant role in the whole reaction system to form the TNCuPc/TiO_2 hierarchical nanofibers.

dx.doi.org/10.1021/am100989a |*ACS Appl. Mater. Interfaces* 2011, 3, 369–377

3.8. Photocatalytic Activity. The photocatalytic degradation of rhodamine B(RB) had been chosen as a model reaction to evaluate the photocatalytic activities of the TNCuPc/TiO_2 hierarchical nanostructures. In the experiments, pure TiO_2 nanofibers (T0) and TNCuPc (P0) were used as a photocatalytic reference to study the photocatalytic activity of the TNCuPc/TiO_2 hierarchical nanostructures. The degradation efficiency of the as-prepared samples was defined as C/C_0, where C and C_0 stood for the remnants and initial concentration of RB, respectively. As observed in Figure 8A, the control experiments were performed under different conditions: (1) in the presence of photocatalysts but in the dark and (2) with visible-light irradiation but in the absence of the photocatalysts. These results illuminated that the adsorption−desorption equilibrium of RB in the dark was established within 30 min. And, there was no appreciable degradation of RB after 4 h in the absence of photocatalysts. Figure 8B shows the degradation curves of RB on the TiO_2 nanofibers (T0), TNCuPc (P0), and TNCuPc/TiO_2 hierarchical nanostructures (PT1 and PT2). As observed in Figure 8B, because of the large band gap energy (3.2 eV for anatase), TiO_2 nanofiber photocatalysis proceeds only at wavelengths shorter than approximately 400 nm. So, TiO_2 nanofibers had a low photocatalytic activity under visible light, and the degradation was only 9% in 4 h. For the TNCuPc/TiO_2 hierarchical nanostructures (PT1), the degradation rate only reached 38% in 4 h, although much higher than pure TiO_2 nanofibers (9%), which might be due to the low TNCuPc loading percentage. In contrast, when the molar ratio of TNCuPc and TiO_2 in the TNCuPc/TiO_2 hierarchical nanostructures increased from 1:50 (PT1) to 1:20 (PT2), the TNCuPc/TiO_2 hierarchical nanostructures (PT2) exhibited the highest photocatalytic activity. The corresponding degradation rates of RB reached about 87% within 4 h, which illuminated that the increase in TNCuPc content obviously enhanced the photocatalytic activity of TNCuPc/TiO_2 hierarchical nanostructures. The photocatalytic activity of pure TNCuPc (P0) was also investigated, which was a little better than that of the pure nanofibers and the corresponding degradation ratio reached 28%. All above experimental results suggested that TNCuPc as visible-light sensitization improve the visible-light photocatalytic activity of the TNCuPc/TiO_2 hierarchical nanostructures. To verify whether hydroxyl radicals (OH•) are involved in the degradation of RB, the photocatalytic degradation of RB was carried out in the presence of tert-butyl alcohol (TBA), a widely used OH• scavenger.[38] As observed in Figure 8C, the presence of TBA greatly depressed the photocatalytic degradation rate of RB on PT2. The relevant degradation ratio was decreased from 87 to 54%. The above TBA experiments confirm the OH• radicals was produced in the presence of TNCuPc/TiO_2 photocatalysts. In other words, the OH• radicals responsible for the observed enhancement in the photocatalytic degradation rate of RB. Moreover, Figure 8D showed the photocatalytic degradation of RB over TNCuPc/TiO_2 hierarchical nanostructures (PT2) under visible-light irradiation with three time cycling uses. It was indicated that those nanofiber photocatalysts with high photocatalytic activity could be easily recovered by sedimentation, and would greatly promote their industrial application to eliminate the organic pollutants from wastewater.

On the basis of the above results and the earlier reports on the dye-sensitized photocatalytic oxidation of pollutants, a proposed mechanism of visible light-induced photodegradation of RB with the TNCuPc/TiO_2 hierarchical nanostructures was elucidated schematically in Scheme 1. The phthalocyanines in the solid state behave as p-type semiconductors, characterized by energy of the band gap about 2 eV.[39−43] Upon irradiation with light $\lambda > 400$ nm, it is possible to excite only the phthalocyanine particles supported on TiO_2 nanofibers and generated the $^1O_2$ via energy transfer (eqs 1 and 2)

Scheme 1. Postulate Mechanism of the Visible-Light-Induced Photodegradation of RB with TNCuPc/TiO_2 Hierarchical Nanostructures

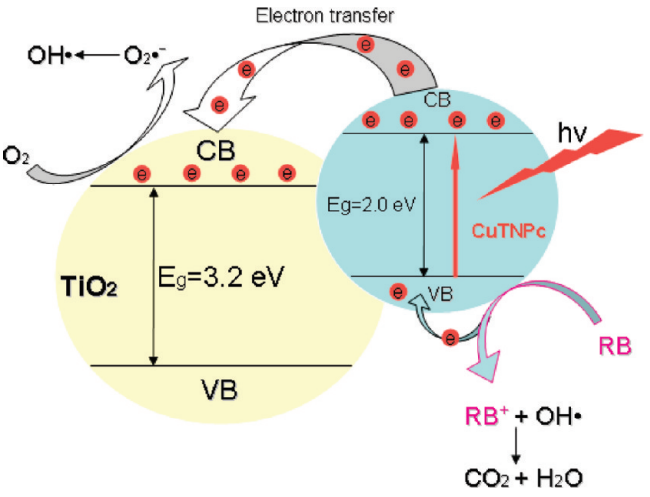

$$\text{dye} + h\nu \rightarrow \text{dye}^* \quad (1)$$

$$\text{dye}^* + O_2 \rightarrow \text{dye} + {}^1O_2 \quad (2)$$

The excited charge is then injected from the excited state of the dye into the conduction band of TiO_2, followed by generation of the dye cationradical (dye•$^+$) and conduction band electrons (e_{cb}^-) of TiO_2 (eq 3).

$$\text{dye}^* + TiO_2 \rightarrow \text{dye}^{\bullet +} + TiO_2(e_{cb}^-) \quad (3)$$

Dissolved oxygen molecules and singlet oxygen ($^1O_2$) reacted with conduction band electrons (e_{cb}^-) to yield superoxide radical anions ($O_2^{\bullet -}$), which on protonation generated the hydroperoxy radicals (HO_2•), producing hydroxyl radicals (OH•) (eqs 4−8), which is a strong oxidizing agent to decompose the organic dye (eq 9)

$$TiO_2(e_{cb}^-) + O_2 \rightarrow TiO_2 + O_2^{\bullet -} \quad (4)$$

$$TiO_2(e_{cb}^-) + {}^1O_2 \rightarrow TiO_2 + O_2^{\bullet -} \quad (5)$$

$$O_2^{\bullet -} + H_2O \rightarrow HO_2\bullet + OH^- \quad (6)$$

$$HO_2\bullet + H_2O \rightarrow H_2O_2 + OH\bullet \quad (7)$$

$$H_2O_2 \rightarrow 2OH\bullet \quad (8)$$

$$OH\bullet + RB \rightarrow CO_2 + H_2O \quad (9)$$

Because the dye•$^+$ radicals has a redoxpotential of about 1.2 V vs NHE,[44,45] it could oxidize a suitable substrate (R), together with

recovery of the original dye (eq 10).

$$\text{dye}^{\bullet+} + \text{RB} \rightarrow \text{dye} + \text{RB}^{\bullet+} \quad (10)$$

In other words, the TiO_2 nanofibers functions as an electron trap for the excited surface adsorbed TNCuPc dye. The trapped electron subsequently induces the generation of active oxygen species. Besides the active oxygen species, the by-produced $TNCuPc^{\bullet+}$ radical cation also reacted with RB and induces the photo degradation of RB. Because no valence band hole is produced in the TiO_2 nanofibers, the interior charge recombination is avoided in the TNCuPC/TiO_2 hierarchical nanostructures. In this cycle, TiO_2 acts only as an electron mediator, and the dye as a sensitizer.

CONCLUSIONS

In summary, by using solvothermal process and electrospinning technology, the TNCuPC/TiO_2 hierarchical nanostructures with novel architectures were successfully fabricated. Moreover, the morphologies of secondary TNCuPc nanostructures could be facilely tuned from nanowires to nanoflowers by adjusting the experimental parameters. And, it is suggested there might probably exist the interaction between TNCuPc and TiO_2.The investigation of photocatalytic ability indicated that the TNCuPC/TiO_2 hierarchical nanostructures exhibited enhanced photocatalytic activity in the decomposition of RB under visible-light ($\lambda > 400$ nm) irradiation. Furthermore, these TNCuPC/TiO_2 hierarchical nanostructures could be easily recycled without decrease of the photocatalytic activity because of their one-dimensional nanostructure property. Also, it is expected that the TNCuPC/TiO_2 hierarchical nanostructures with high photocatalytic activity will greatly promote their industrial application to eliminate the organic pollutants from wastewater.

AUTHOR INFORMATION

Corresponding Author

*E-mail: clshao@nenu.edu.cn. Tel. 8643185098803.

ACKNOWLEDGMENT

The present work is supported financially by the National Natural Science Foundation of China (50572014, 50972027, and 10647108) and the Program for New Century Excellent Talents in University (NCET-05-0322).

REFERENCES

(1) Fujishima, A.; Rao, T. N.; Tryk, D. A. *J. Photochem. Photobiol., C* **2000**, *1*, 1.
(2) Kamat, P. V. *Chem. Rev.* **1993**, *93*, 267.
(3) Hoffmann, M. R.; Martin, S. T.; Choi, W.; Bahnemann, D. W. *Chem. Rev.* **1995**, *95*, 69.
(4) Linsebigler, A.; Lu, G.; Yates, J. T. *Chem. Rev.* **1995**, *95*, 735.
(5) Wang, C.; Li, J.; Mele, G.; Duan, M. Y.; Lü, X. F.; Palmisano, L.; Vasapollo, G.; Zhang, F. X. *Dyes Pigm.* **2010**, *84*, 183.
(6) Woolerton, T. W.; Sheard, S.; Reisner, E.; Pierce, E.; Ragsdale, S. W.; Armstrong, F. A. *J. Am. Chem. Soc.* **2010**, *132*, 2133.
(7) Reisner, E.; Powell, D. J.; Cavazza, C.; Fontecilla-Camps, J. C.; Armstrong, F. A. *J. Am. Chem. Soc.* **2009**, *131*, 18466.
(8) Kisch, H.; Zang, L.; Lange; Maier, W. F.; Antonis, C.; Meissner, D. *Angew. Chem., Int. Ed.* **1998**, *37*, 3034.
(9) Zhao, D.; Chen, C. C.; Wang, Y. F.; Ma, W. H.; Zhao, J. C.; Rajh, T.; Zang, L. *Environ. Sci. Technol.* **2008**, *42*, 314.
(10) Zhang, J.; Bang, J. H.; Tang, C.; Kamat, P. V. *ACS Nano* **2010**, *4*, 387.
(11) Huang, L.; Peng, F.; Wang, H.; Yu, H.; Li, Z. *Catal. Commun.* **2009**, *10*, 1839.
(12) Zhou, W. J.; Liu, H.; Wang, J. Y.; Liu, D.; Du, G. J.; Cui, J. J. *ACS Appl. Mater. Interfaces* **2010**, *2*, 2385.
(13) Yu, J. C.; Wu, L.; Lin, J.; Li, P. S.; Li, Q. *Chem. Commun* **2003**, 1552.
(14) Zhang, Z. Y.; Shao, C. L.; Zhang, L. N.; Li, X. H.; Liu, Y. C. *J. Colloid Interface Sci.* **2010**, *351*, 57.
(15) Yu, H. G.; Irie, H.; Shimodaira, Y.; Hosogi, Y.; Kuroda, Y.; Miyauchi, M.; Hashimoto, K. *J. Phys. Chem. C* **2010**, *114*, 16481.
(16) Karunakaran, C.; Abiramasundari, G.; Gomathisankar, P.; Manikandan, G.; Anandi, V. *J. Colloid Interface Sci.* **2010**, *352*, 68.
(17) Fuerte, A.; Hernandez-Alonso, M. D.; Maira, A. J.; Martinez-Arias, A.; Fernandez-Garcia, M.; Coneasa, J. C.; Soria, J. *Chem. Commun.* **2001**, 2718.
(18) Kato, H.; Kudo, A. *J. Phys. Chem. B* **2002**, *106*, 5029.
(19) Etacheri, V.; Seery, M. K.; Hinder, S. J.; Pillai, S. C. *Chem. Mater.* **2010**, *22*, 3843.
(20) Pelaeza, M.; Falarasb, P.; Likodimosb, V.; Kontosb, A. G.; Cruzc, A. A.; O'shead, K.; Dionysiou, D. D. *Appl. Catal., B* **2010**, *993*, 78.
(21) Zhong, J.; Chen, F.; Zhang, J. L. *J. Phys. Chem. C* **2010**, *114*, 933.
(22) Wang, J.; Tafen, D.; Lewis, J. P.; Hong, Z. L.; Manivannan, A.; Zhi, M. J.; Li, M.; Wu, N. Q. *J. Am. Chem. Soc.* **2009**, *131*, 12297.
(23) Wang, Z. Y.; Mao, W. P.; Chen, H. F.; Zhang, F.; Fan, X. P.; Qian, G. D. *Catal. Commun.* **2006**, *7*, 518.
(24) Chen, F.; Deng, Z. G.; Li, X. P.; Zhang, J. L.; Zhao, J. C. *Chem. Phy. Lett.* **2005**, *415*, 85.
(25) Sun, Q.; Xu, Y. M. *J. Phys. Chem. C* **2009**, *113*, 12387.
(26) Fa, W. J.; Zan, L.; Gong, C. Q.; Zhong, J. C.; Deng, K. J. *Appl. Catal., B* **2008**, *79*, 216.
(27) Zhao, Z. H.; Fan, J. M.; Xie, M. M.; Wang, Z. Z. *J. Cleaner Prod.* **2009**, *17*, 1025.
(28) Rajić, N. Z.; Stojaković, D. R. *J. Coord. Chem.* **1989**, *19*, 291.
(29) Edwards, L.; Gouterman, M. *J. Mol. Spectrosc.* **1970**, *33*, 292.
(30) Nozawa, T. *Biochim. Biophys. Acta* **1980**, *626*, 282.
(31) Nykong, T.; Gasyna, Z.; Stillman, M. J. *Inorg. Chem.* **1987**, *26*, 1087.
(32) VanCott, T. C.; Rose, J. L.; Misener, G. C.; Williamson, B. E.; Schrimpf, A. E.; Boyle, M. E.; Schatz, P. N. *J. Phys. Chem.* **1989**, *93*, 2999.
(33) Seoudi, R.; El-Bahy, G. S.; El Sayed, Z. A. *J. Mol. Struct.* **2005**, *753*, 119.
(34) Kobayashi, T.; Kondo, R.; Nakajima, S. J. *Spectrochim. Acta* **1970**, *26 A*, 1305.
(35) Jarosz, G.; Quinn, P. D.; Stephan, N.; Brehmer, L. *Thin Solid Films* **2005**, *474*, 301.
(36) Karimov, K. S.; Qazi, I.; Khan, T. A; Draper, P. H.; Khalid, F. A.; Mahroof-Tahir, M. *Environ. Monit. Assess.* **2008**, *141*, 323.
(37) Schwarz, P. F.; Turro, N. J.; Bossmann, S. H.; Braun, A. M.; Wahab, A. M. A. A.; Durr, H. *J. Phys. Chem. B* **1997**, *101*, 7127.
(38) Lv, K. L.; Xu, Y. M. *J. Phys. Chem. B* **2006**, *110*, 6204.
(39) Schlettwein, D.; Kaneko, M.; Yamada, A.; Wöhrle, D.; Jaeger, N. I. *J. Phys. Chem.* **1991**, *95*, 1748.
(40) Loutfy, R. O.; Sharp, J. H. *J. Chem. Phys.* **1979**, *71*, 1211.
(41) Tang, C. W. *Appl. Phys. Lett.* **1986**, *48*, 183.
(42) Popovic, Z. D. *Chem. Phys.* **1984**, *86*, 311.
(43) Iliev, V. *J. Photochem. Photobiol. Chem.* **2002**, *151*, 195.
(44) Darwent, J. R.; Douglas, P.; Harriman, A.; Porter, G.; Richoux, M. C. *Coord. Chem. Rev.* **1982**, *44*, 83.
(45) Hodak, J.; Quinteros, C.; Litter, M. I.; Roman, E. S. *J. Chem. Soc., Faraday Trans.* **1996**, *92*, 5081.